

## Explicit Water Models Affect the Specific Solvation and Dynamics of Unfolded Peptides While the Conformational Behavior and Flexibility of Folded Peptides Remain Intact

Petra Florová, Petr Sklenovský, Pavel Banáš, and Michal Otyepka\*

*Regional Centre of Advanced Technologies and Materials, Department of Physical Chemistry, Faculty of Science, Palacký University Olomouc, tr. 17 listopadu 12, 771 46 Olomouc, Czech Republic*

Received June 30, 2010

**Abstract:** Conventional molecular dynamics simulations on 50 ns to 1  $\mu$ s time scales were used to study the effects of explicit solvent models on the conformational behavior and solvation of two oligopeptide solutes:  $\alpha$ -helical EK-peptide (14 amino acids) and a  $\beta$ -hairpin chignolin (10 amino acids). The widely used AMBER force fields (ff99, ff99SB, and ff03) were combined with four of the most commonly used explicit solvent models (TIP3P, TIP4P, TIP5P, and SPC/E). Significant differences in the specific solvation of chignolin among the studied water models were identified. Chignolin was highly solvated in TIP5P, whereas reduced specific solvation was found in the TIP4P, SPC/E, and TIP3P models for kinetic, thermodynamic, and both kinetic and thermodynamic reasons, respectively. The differences in specific solvation did not influence the dynamics of structured parts of the folded peptide. However, substantial differences between TIP5P and the other models were observed in the dynamics of unfolded chignolin, stability of salt bridges, and specific solvation of the backbone carbonyls of EK-peptide. Thus, we conclude that the choice of water model may affect the dynamics of flexible parts of proteins that are solvent-exposed. On the other hand, all water models should perform similarly for well-structured folded protein regions. The merits of the TIP3P model include its high and overestimated mobility, which accelerates simulation processes and thus effectively increases sampling.

### Introduction

Molecular dynamic (MD) simulations of biomacromolecules are based on empirical force fields, which relate potential energy and molecular structure. Several in-depth overviews of current trends in the field of empirical potentials have been published.<sup>1–5</sup> Among all of the available empirical potentials, the AMBER,<sup>6,7</sup> GROMOS,<sup>8</sup> CHARMM,<sup>9</sup> and OPLS<sup>10</sup> families of force fields have performed well for biomacromolecules. However, in this study we deal only with the AMBER family of force fields, which have been thoroughly tested on a variety of biomolecular systems. The AMBER family of force fields perform well for a range of

systems including proteins,<sup>11</sup> RNA,<sup>12</sup> and DNA<sup>13,14</sup> and their homo- and heterocomplexes.<sup>15</sup>

One of the AMBER force fields is ff99 (also referred to as parm99),<sup>16</sup> which is a second-generation force field based on the Cornell et al. set of effective parameters<sup>17</sup> employing the pair-additive potential used for condensed-phase all-atomic simulations. Simmerling et al. have shown that the ff99 force field does not accurately represent glycine behavior in protein simulations and that it is prone to other inaccuracies, including overstabilization of  $\alpha$ -helical peptide conformations and underestimation of  $\beta$ -bend propensity.<sup>18</sup> Simmerling et al. also suggested a reparametrization of backbone torsion terms, yielding the modified force field ff99SB,<sup>18</sup> which improved the balance in secondary structure propensities. A third-generation AMBER force field, ff03,

\* Corresponding author e-mail: michal.otyepka@upol.cz.

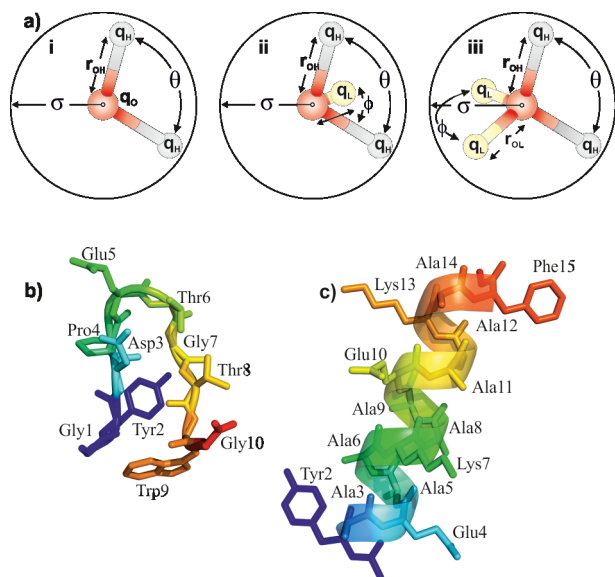


**Figure 1.** (a) Three-dimensional representations of three-site TIP3P and SPC/E (left), four-site TIP4P (middle), and five-site TIP5P (right) water models. The labels correspond to the parameters listed in Table 1. (b) Chignolin and (c) EK-peptide structures in stick representations.

was introduced by Duan et al., who revised all  $\psi/\phi$  torsion parameters and recalculated atomic partial charges.<sup>19</sup> Despite such efforts, none of these recent force fields are perfect; for example, Hummer et al. showed that ff03 overestimated and ff99SB underestimated  $\alpha$ -helical propensities.<sup>20,21</sup>

The quest for a sufficiently accurate force field has mainly focused on solute behavior, with only marginal consideration of the water environment. However, the water environment plays an essential role in biomolecular processes, and some important effects, such as the hydrophobic effect and Coulomb interaction screening, vanish if the water molecules do not surround a biomolecule.<sup>22–25</sup> An explicit consideration of water molecules is therefore essential for a reasonably accurate description of, at least, solute–solvent interactions.<sup>26</sup> A large number of explicit water models have been developed in attempts to accommodate all of the physico-chemical properties of water.<sup>27–37</sup> Among them, Jorgensen's TIP3P<sup>28,29,38</sup> and Berendsen's SPC/E<sup>39</sup> models (Figure 1, Table 1) are the most widely used for biomolecular simulations. It should be noted, however, that although these explicit solvent models have been derived to represent the physico-chemical properties of bulk water well, i.e., their solvent–solvent interactions, the balance of solute–solvent interactions in these models remains questionable and requires further study.

All of the popular TIP3P and SPC/E water models agree well with bulk water characteristics at ambient temperatures. The three-site TIP3P model (in which point charges are centered on each of the three atoms) is the most commonly used model in AMBER simulations. TIP3P reproduces well the key features of bulk water at 25 °C and 1 atm (i.e., a density of 0.997 g/cm<sup>3</sup> and heat of vaporization of 10.53 kcal/mol), but it underestimates the height of the second (tetrahedral) peak in the O–O radial distribution function and overestimates the diffusion constant (Table 1). Both the four-site TIP4P and five-site TIP5P models give better fits

to the experimental O–O radial distribution function and also behave better than the TIP3P model in many other respects. However, improving the representation of water properties by adding additional extra point charges increases computational costs considerably, with TIP4P being approximately 1.5 times and TIP5P 2.5 times as expensive as TIP3P in terms of the simulation time (Table 1). The original three-site SPC water model has been superseded by the SPC/E model, which includes corrections for self-polarization and improved structural and diffusion properties. The computational demands of the SPC/E model are comparable to those of the TIP3P model.

Despite the development of sufficiently representative force fields and explicit water models, less attention has been paid to the effects of explicit water models on solute behavior, namely, on the structure, dynamics, and kinetics of solute molecules. Moreover, explicit water models differ in ways that are likely to generate differences in solute–solvent interactions, which might then propagate to differences in solute behavior in various explicit solvent models. In response to the call for studies on the effects of explicit water models on solute behavior reported in the literature,<sup>1,40–43</sup> Nutt and Smith presented CHARMM simulations of *N*-methylacetamide, other small solute molecules, and a small protein (crabrin) in various solvent models, concluding that although TIP3P, TIP4P, and TIP5P differed in solute–solvent interactions, they provided similar overall descriptions of solvation.<sup>40</sup> However, their results on biomacromolecular solute behavior were, unfortunately, limited by their use of only a 2–3 ns time scale and of an alternative modified TIP3P solvent model (mTIP3P; bearing modified van der Waals parameters for hydrogen,  $\sigma_{HH} = 0.449$  Å and  $\epsilon_H = 0.046$  kcal/mol).<sup>44</sup> In a recent study, Vymětal and Vondrášek studied the effects of different explicit water models on the free energy  $\phi$ – $\psi$  profiles of alanine dipeptide using metadynamics. They concluded that the choice of solvent model had no significant effect on the conformational preferences of alanine dipeptide.<sup>45</sup> Molecular dynamics simulations of small proteins carried out by Wong and Case in ff99SB showed that protein diffusion occurs rapidly due to the high self-diffusion constant of TIP3P, whereas the SPC/E and TIP4P water models with more realistic self-diffusion constants have too large a protein rotation diffusion constant.<sup>42</sup> Shirts et al. calculated hydration free energies of the amino acid side chain analogues in several water models and concluded that modified TIP3P (TIP3P-MOD; having different  $\sigma_O = 3.12171$  Å and  $\epsilon_O = 0.190$  kcal/mol parameters compared to the standard TIP3P parameters; see Table 1)<sup>46</sup> gave the closest match to the experimental data. On the other hand, the ability of explicit solvent models to accurately represent pure water properties did not necessarily determine the ability to correctly predict solute/solvent behavior.<sup>41,47</sup>

In the present study we examine the structure and dynamics of the small peptide solutes chignolin and EK-peptide (Figure 1) in MD simulations on 50 ns to 1  $\mu$ s time scales (20.7  $\mu$ s in total). Chignolin is an artificial peptide consisting of 10 residues (GYDPETGTWG) which adopts a  $\beta$ -hairpin conformation in solution under in vitro conditions (Figure 1b). The peptide is stabilized by H-bonds between

**Table 1.** Parameters and Physicochemical Properties of the Explicit Water Models Studied, As Used in the AMBER Package<sup>a</sup>

param (units)	TIP3P	TIP4P	TIP5P	SPC/E	exptl
$q_H^b$ (e)	0.417	0.520	0.241	0.424	
$q_O^b$ (e)	-0.834	0.000	0.000	-0.848	
$q_L^b$ (e)		-1.040	-0.241		
$r_{OH}^c$ (Å)	0.9572	0.9572	0.9572	1.0000	0.9572 <sup>76</sup>
$r_{OL}^c$ (Å)		0.1500	0.7000		
$\theta_{HOH}^d$ (deg)	104.520	104.520	104.520	109.470	104.474 <sup>76</sup>
$\phi_{LOL}^d$ (deg)			109.470		
$\varepsilon^e$ (kcal/mol)	0.1521	0.1550	0.1600	0.1554	
$\sigma_O^e$ (Å)	3.1506	3.1537	3.1200	3.1656	
cost <sup>f</sup>	100	140	240	100	
dipole moment (D)	2.35 <sup>28</sup>	2.18 <sup>30</sup>	2.29 <sup>28</sup>	2.35 <sup>30</sup>	2.95 <sup>77</sup>
dielectric constant	82.0 <sup>30</sup>	53.0 <sup>30</sup>	81.5 <sup>28</sup>	71.0 <sup>30</sup>	78.4 <sup>78</sup>
density(298 K, 1 atm) (g/cm <sup>3</sup> )	0.986 ± 0.010 <sup>g</sup>	0.994 ± 0.010 <sup>g</sup>	0.985 ± 0.010 <sup>g</sup>	0.999 ± 0.010 <sup>g</sup>	0.997
self-diffusion(298 K, 1 atm) (10 <sup>-5</sup> cm <sup>2</sup> /s)	5.5 <sup>g</sup>	3.5 <sup>g</sup>	2.7 <sup>g</sup>	2.5 <sup>g</sup>	2.3 <sup>50</sup>
density maximum (K)	~182.15 <sup>31</sup>	~248.15 <sup>28</sup>	~277.15 <sup>28</sup>	~235.15 <sup>32</sup>	277.134 <sup>79</sup>
melting temperature (K)	145.55 <sup>32</sup>	232.45 <sup>32</sup>	273.95 <sup>32</sup>	214.95 <sup>32</sup>	273.15

<sup>a</sup> See Figure 1. <sup>b</sup>  $q_H$ ,  $q_O$ , and  $q_L$  are the partial charges of hydrogen and oxygen and that on the lone pair, respectively. <sup>c</sup>  $r_{OH}$  and  $r_{OL}$  are the oxygen-hydrogen and oxygen-lone pair distances, respectively. <sup>d</sup>  $\theta_{HOH}$  and  $\phi_{LOL}$  are the hydrogen-oxygen-hydrogen and lone pair-oxygen-lone pair angles, respectively. <sup>e</sup>  $\varepsilon$  and  $\sigma$  are the well depth and van der Waals radius Lennard-Jones parameters, respectively. <sup>f</sup> Computer cost in percent with respect to TIP3P. <sup>g</sup> Data from this study.

**Table 2.** List of Simulations Performed for Each Studied System

system		no. of simulations run in tested force fields		
		ff99	ff99SB	ff03
chignolin	TIP3P	6 × 100 ns; 1 × 1 μs	6 × 50 ns; 1 × 1 μs	6 × 50 ns; 1 × 1 μs
	TIP4P	6 × 50 ns	6 × 50 ns	6 × 50 ns
	TIP5P	6 × 50 ns	6 × 50 ns	6 × 50 ns
	SPC/E	6 × 100 ns; 1 × 1 μs	6 × 50 ns; 1 × 1 μs	6 × 50 ns; 1 × 1 μs
EK-peptide	TIP3P	6 × 100 ns; 1 × 1 μs	6 × 50 ns; 1 × 1 μs	6 × 100 ns; 1 × 1 μs
	TIP4P	6 × 50 ns	6 × 50 ns	6 × 50 ns
	TIP5P	6 × 50 ns	6 × 50 ns	6 × 50 ns
	SPC/E	6 × 100 ns; 1 × 1 μs	6 × 50 ns; 1 × 1 μs	6 × 50 ns; 1 × 1 μs

atoms Asp3(O) and Gly7(N) (the strongest), Asp3(N) and Thr8(O), and Asp3(O<sup>δ</sup>) and Glu5(N). Gly7 plays a further key role in chignolin structure stability because its left-handed  $\alpha$ -helical conformation enables propagation of the C-terminal strand. It has been suggested that the side chain interaction between Tyr2 and Trp9 also stabilizes chignolin. The experimental data concerning chignolin stability suggest that the peptide has a ratio of folded to unfolded states equal to ~60:40 at 300 K.<sup>48</sup> EK-peptide is an artificial 14 residue long  $\alpha$ -helix (YAEAAKAAEAAKAF).<sup>49</sup> An  $\alpha$ -helicity of 40% at 273 K was measured for EK-peptide using circular dichroism (CD) spectroscopy. Ghosh and Dill found that the  $\alpha$ -helicity of EK-peptides generally decreases with increasing temperature and amounts to ~20% at 300 K for the studied EK-peptide.<sup>50</sup> In the present study, four explicit solvent models (TIP3P, TIP4P, TIP5P, and SPC/E) combined with three AMBER family force fields (ff99, ff99SB, and ff03) are analyzed to elucidate the role of explicit solvent models on the behavior of both oligopeptides.

## Methods

**Studied Systems.** A designed  $\beta$ -hairpin peptide, chignolin, and an artificial  $\alpha$ -helical EK-peptide were chosen as test systems for the MD simulations. The chignolin NMR structure (PDB ID 1UAO) was used as a starting structure in MD simulations, and both chignolin termini were charged

(N-terminus positively and C-terminus negatively) in all MD simulations. The starting structure of EK-peptide was modeled as an  $\alpha$ -helix in accordance with CD spectra.<sup>49</sup> Although, to our best knowledge, no structural data such as X-ray or NMR spectra are available for EK-peptide, the data from CD spectra are sufficient to provide relevant information about its structure. The N-terminus of EK-peptide was capped by an acetyl group and the C-terminus by *N*-methanamide for MD simulations.

**Molecular Dynamics Simulations.** All MD simulations were carried out using the AMBER suite of programs with the all-atomic force fields ff99,<sup>16</sup> ff99SB,<sup>18</sup> and ff03.<sup>19</sup> The simulation protocol, which has been repeatedly shown to perform well for proteins,<sup>51–55</sup> was set up as follows. The hydrogen atoms were added by the LEaP module of AMBER. Systems were then neutralized by adding counterions (Na<sup>+</sup> or Cl<sup>-</sup>, according to the solute charge) and immersed into a rectangular box of explicit water molecules. Each system was solvated by four explicit water models—TIP3P, TIP4P, TIP5P, and SPC/E (Table 1). The initial coordinates of solute, as well as solvent, atoms were identical for a given peptide system in all water models and all force fields. Consequently, we examined the systems' dynamics in all 12 possible combinations of solute force field and solvent type (Table 2). In each simulation, the minimal distance between the solute and the box wall was set to

10 Å. Prior to the production phase of the MD run, each system was minimized by first optimizing the positions of the hydrogen atoms while the heavy atoms remained constrained; then all protein atoms were constrained, and the solvent molecules with counterions were allowed to move during a 1000-step minimization, followed by 10 ps long MD runs under  $[NpT]$  conditions ( $p = 1$  atm,  $T = 298.16$  K). After this, the side chains were relaxed by several minimization runs, with decreasing force constants applied to the backbone atoms. After the relaxation, each system was heated from 10 to 298.16 K for 100 ps. The particle-mesh Ewald (PME) method was used for treating electrostatic interactions, and all simulations were performed under periodic boundary conditions in the  $[NpT]$  ensemble at 298.16 K and 1 atm using a 2 fs integration step. The SHAKE algorithm, with a tolerance of  $10^{-5}$  Å, was used to fix the positions of all hydrogen atoms, and a 9.0 Å cutoff was applied to nonbonding interactions. The Berendsen thermostat was used.<sup>56</sup>

All systems studied are listed in Table 2. Generally, the dynamics of each system in respective combinations of solute–solvent description were modeled via six MD simulations on 50–100 ns time scales, in which the coordinates were stored every picosecond. The number of parallel MD simulations in each run was chosen according to Day and Daggett,<sup>57</sup> who suggested that, for capturing average properties of simulated systems, 5–10 simulations in multiple MD runs are sufficient. Moreover, additional extensive 1  $\mu$ s long MD runs with coordinates stored every 10 ps were performed for all force fields in combinations with the TIP3P and SPC/E models. The total simulation time in the present study (the sum of the simulation times of all systems) reached 20.7  $\mu$ s.

In addition to the peptide simulations, we carried out water box simulations (i.e., only water molecules without solute) for the TIP3P, TIP4P, TIP5P, and SPC/E models under  $[NpT]$  conditions ( $p = 1$  atm,  $T = 298.16$  K) and using an 8.0 Å cutoff for nonbonding interactions on 10 ns time scales. A periodic rectangular cubic box with dimensions of  $20 \times 20 \times 20$  Å filled with 375 explicit water molecules was used in each water box simulation.

**Analyses of Trajectories.** The  $\alpha$ -helix dynamics were monitored using the secondary structure analysis (implemented in ptraj from the AMBER package), the time evolution of the root-mean-square deviations (rmsd's) of the backbone atoms (C, N, C $_{\alpha}$ ) with respect to the initial structure, and the time evolution of the distances between atoms forming salt bridges (Glu3(C $_{\delta}$ )–Lys6(N $_{\epsilon}$ ), Lys6(N $_{\epsilon}$ )–Glu9(C $_{\delta}$ ), and Glu9(C $_{\delta}$ )–Lys12(N $_{\epsilon}$ )). The numbers of water molecules in the first solvation shell (<3.4 Å) around the carbonyl oxygen of each residue were calculated for ff03 EK-peptide simulations using ptraj. The  $\alpha$ -helix was said to be unfolded if there were fewer than four neighboring helical residues for more than 100 ps (in accordance with Daggett<sup>58</sup>). The following structural analyses for chignolin simulations were performed: the time evolution of the rmsd's of the backbone atoms (C, N, C $_{\alpha}$ ) from the initial structure and the distances between C $_{\gamma}$  atoms of Tyr2 and Trp9. In this study, all structures with an rmsd of main chain atoms up to 1.7 Å were considered to be native-like, because all

chignolin structures from the NMR ensemble fitted into this interval. In addition, structures from the MD ensemble with rmsd below 1.7 Å displayed a native H-bond network and native distance between Tyr2 and Trp9 (C $_{\gamma}$  atoms). We considered the chignolin molecule as unfolded if the rmsd of the backbone atoms was above 1.7 Å for more than 100 ps.

The effect of water models on the unfolding or refolding rates in ff99 chignolin simulations were analyzed by the following statistical model. Unfolding and refolding are stochastic processes having Bernoulli distributions with associated probabilities  $p_{\text{unfold}}$  and  $p_{\text{refold}}$ . The  $p_{\text{unfold}}$  probability can be estimated from the number of unfolding events (within a 1 ps time frame) divided by the number of snapshots where the system was folded. Similarly, the estimate of  $p_{\text{refold}}$  equals the number of refolding events divided by the number of snapshots where the system is unfolded. These estimates have a binomial distribution, which can be approximated by a normal distribution, and thus, the confidence intervals documenting statistical relevance of these estimated probabilities can be expressed by the Wilson score interval:<sup>52</sup>

$$p_{\min, \max} = \frac{p + \frac{1}{2n} z_{1-\alpha/2}^2 \pm \sqrt{\frac{p(1-p)}{n} + \frac{z_{1-\alpha/2}^2}{4n^2}}}{1 + \frac{1}{n} z_{1-\alpha/2}^2}$$

where  $p$  is the estimated probability,  $p_{\min}$  and  $p_{\max}$  are the lower and upper limits of the Wilson score interval of the estimated probability,  $n$  is the number of realizations (i.e., total number of snapshots) where the system is folded/unfolded, and  $z_{1-\alpha/2}$  is the  $1 - \alpha/2$  percentile of the normal distribution (the  $\alpha$  value used was 5%). Finally, the corresponding kinetic constants ( $k_{\text{unfold/refold}}$ ) were derived from the estimated probabilities of unfolding and refolding ( $p_{\text{unfold/refold}}$ ) using the first-order kinetic equation

$$P_{\text{unfold/refold}} = \exp(-k_{\text{unfold/refold}} \Delta t)$$

where  $\Delta t$  denotes the time interval between two consecutive snapshots. Subsequently, these kinetic constants were transformed to the corresponding potential free energy barriers ( $\Delta G_{\text{unfold/refold}}^{\ddagger}$ ) using the Eyring equation

$$k_{\text{unfold/refold}} = \left( \frac{k_B T}{h} \right) \exp \left( - \frac{\Delta G_{\text{unfold/refold}}^{\ddagger}}{RT} \right)$$

in which  $T$  is the absolute temperature and  $k_B$ ,  $R$ , and  $h$  are the Boltzmann, universal gas, and Planck constants, respectively.

The population and evolution of chignolin conformations in various water models in the ff99 simulations were monitored by the Bayesian clustering algorithm<sup>59</sup> implemented in ptraj, with all variables set to the default (i.e., without the critical distance metric). The optimal cluster number was found iteratively with visual inspection of indices measuring the clustering performance.

The Ramachandran plots of peptide residues were depicted as scatter plots and density plots using an in-house script. The names of canonical regions and their positions in the Ramachandran plot were assigned according to Schlick.<sup>60</sup>



The following analyses of specific solvation in various solvents were performed only for ff99SB chignolin simulations, given the sufficient stability of chignolin in ff99SB; density maps of water models were calculated using ptraj (grid analysis). Prior to the analysis, chignolin was image-centered and rms-fitted, and then finally the density of water molecules was calculated using cubic grids spread over the entire box volume. The output file was visualized using VMD. Further, the numbers of water molecules in the first and second solvation shells around the chignolin molecule were calculated using ptraj. The distance of the chignolin first hydration shell was set to 3.4 Å and the second to 5.0 Å. The analysis of water residence times on the chignolin surface was based on a survival probability correlation function as implemented in ReTiNaI (Resident Time Analyzer v1.0, Petr Kulhanek, NCBR Brno, <http://troll.chemi.muni.cz/whitezone/development/root/>) software (see ref 61 for details). Water molecules interacting with oxygen or nitrogen atoms of chignolin with residence time over 0.5 ns were further analyzed.

Self-diffusion coefficients (Table 1) were calculated from the last 5 ns of 10 ns long water box simulations using the Einstein equation

$$D = \frac{1}{6tN} \lim_{t \rightarrow \infty} \left\langle \sum_{i=1}^N [r_i(t) - r_i(0)]^2 \right\rangle$$

where  $D$  is the self-diffusion coefficient,  $t$  is time,  $N$  is the total number of atoms, and  $r_i(t)$  is the displacement vector of the  $i$ th atom at time  $t$ . The radial distribution functions of each water model (Figure S1, Supporting Information) were calculated over the entire time scale of the water box simulations by ptraj.

## Results

**Chignolin. ff99 Force Field.** The simulations showed that chignolin did not maintain its native-like structure in the ff99 force field and melted readily in almost all simulations with different solvent models (Table 3). The differences among estimated probabilities and corresponding free energy barriers of unfolding/refolding processes in different solvation models were not statistically significant ( $\alpha = 0.05$ ). Nonetheless, the free energy barriers of unfolding and refolding differed significantly in different force fields, as discussed below (Table 4). The agreement between free energy barriers of unfolding estimated from a series of 100 ns simulations, and from the 1  $\mu$ s long simulation in the TIP3P and SPC/E water models, shows that the simulations sufficiently converged on a 100 ns time scale, in terms of estimation of unfolding probability. On the other hand, this does not apply for the probability of refolding, because, on longer simulation time scales, higher free energy barriers of refolding were in most cases estimated. This could have been a consequence of further structural relaxation of the unfolded state toward some energetically deeper minima.

After chignolin lost its native-like structure, it adopted one of five misfolded conformations (designated clusters 1–5; Figure S2, Supporting Information), which were subsequently identified by a cluster analysis (Table 5). We did not observe

**Table 3.** Populations (%) of the Native-like Chignolin Structures and  $\alpha$ -Helicity (%) of EK-Peptide in the Respective MD Simulations

force field	water model	native-like <sup>a</sup>		$\alpha$ -helicity <sup>b</sup>	
		multiple <sup>c</sup>	long <sup>d</sup>	multiple <sup>c</sup>	long <sup>d</sup>
ff99	TIP3P	18 $\pm$ 26	3	16 $\pm$ 20	15 $\pm$ 20
	TIP4P	24 $\pm$ 26		14 $\pm$ 19	
	TIP5P	53 $\pm$ 36		20 $\pm$ 23	
	SPC/E	36 $\pm$ 35	11	21 $\pm$ 23	17 $\pm$ 21
ff99SB	TIP3P	95 $\pm$ 7	74	21 $\pm$ 26	4 $\pm$ 12
	TIP4P	94 $\pm$ 7		17 $\pm$ 24	
	TIP5P	94 $\pm$ 6		35 $\pm$ 30	
	SPC/E	96 $\pm$ 6	83	20 $\pm$ 29	4 $\pm$ 12
ff03	TIP3P	96 $\pm$ 2	46	70 $\pm$ 22	68 $\pm$ 23
	TIP4P	80 $\pm$ 22		74 $\pm$ 17	
	TIP5P	96 $\pm$ 2		73 $\pm$ 22	
	SPC/E	78 $\pm$ 19	79	79 $\pm$ 15	70 $\pm$ 22

<sup>a</sup> The mean populations of the native chignolin structure with their standard deviations were calculated from multiple simulations. <sup>b</sup> The  $\alpha$ -helicities are mean values with standard deviations, calculated from all multiple MD simulations or from one 1  $\mu$ s run, respectively. <sup>c</sup> Six independent simulations. <sup>d</sup> A 1  $\mu$ s MD simulation.

any significant difference in populations of unfolded clusters between simulations with the TIP3P and TIP4P models. However, the TIP5P model produced simulations significantly different from those of both TIP3P and TIP4P. The cluster 1 conformation, which was the dominant unfolding state in the TIP3P and TIP4P simulations, was hardly populated in the TIP5P simulations. Instead, the cluster 2 conformation was significantly preferred in the TIP5P simulations, but negligible in populations from the TIP3P and TIP4P simulations (Table 5). Note that the cluster 2 conformation, despite being unfolded, retained a left-handed  $\alpha$ -helical conformation of Gly7, which seems to be the critical residue for proper chignolin folding.<sup>48</sup> Both clusters 1 and 2 were occupied in the series of 100 ns simulations with SPC/E, and their populations did not significantly differ from those of any of the TIP $n$ P simulations. When we extended sampling of simulations with TIP3P and SPC/E, the most widely used models, to a 1  $\mu$ s time scale, we found the cluster populations in TIP3P 100 ns simulations were more or less converged, while further relaxation was observed with the SPC/E model. Specifically, cluster 1 became the most populated unfolded state while cluster 2 was no longer observed in 1  $\mu$ s long SPC/E simulations. Thus, chignolin in the SPC/E water model on microsecond time scales occupied the same unfolded clusters as in the TIP3P and TIP4P models, which were, however, significantly different from those clusters populated in the TIP5P model. It is worth noting that the transitions between unfolded clusters happened more rapidly in TIP3P than in the SPC/E model, which seems to be a consequence of the higher self-diffusion coefficient of TIP3P (Table 1) and could be the reason for better convergence of cluster populations in TIP3P 100 ns simulations compared to SPC/E simulations (see Figure S3, Supporting Information).

Ramachandran density and scatter plots revealed that some residues moved apart from the native regions (defined from the NMR structure;<sup>48</sup> Figure S2, Supporting Information) and also populated the non-native ones (Figure S4, Supporting

**Table 4.** Estimated Free Energy Barriers (kcal/mol) of Unfolding ( $\Delta G_{\text{unfold}}^{\ddagger}$ ) and Refolding ( $\Delta G_{\text{refold}}^{\ddagger}$ ) and Corresponding Free Energy Differences (kcal/mol) between Unfolded and Folded States ( $\Delta G = G_{\text{unfold}} - G_{\text{fold}}$ ) of Chignolin in Various Solvent Models and Force Fields (298 K, 1 atm)<sup>a</sup>

force field	water model	$\Delta G_{\text{unfold}}^{\ddagger}$	$\Delta G_{\text{refold}}^{\ddagger}$	$\Delta G$
ff99	TIP3P	6.8 ± 0.4 (6.3 ± 0.5)	8.5 ± 0.8 (8.3 ± 0.5)	-1.7 ± 0.9 (-2.1 ± 0.7)
	TIP4P	6.5 ± 0.4	7.8 ± 0.6	-1.3 ± 0.7
	TIP5P	7.1 ± 0.4	7.3 ± 0.6	-0.2 ± 0.7
	SPC/E	6.7 ± 0.3 (6.9 ± 0.4)	7.2 ± 0.3 (8.2 ± 0.5)	-0.5 ± 0.4 (-1.3 ± 0.6)
ff99SB	TIP3P	7.5 ± 0.5 (7.3 ± 0.3)	5.7 ± 0.5 (6.8 ± 0.3)	1.9 ± 0.7 (0.6 ± 0.4)
	TIP4P	7.4 ± 0.4	5.4 ± 0.4	1.9 ± 0.6
	TIP5P	7.5 ± 0.5	5.5 ± 0.5	2.0 ± 0.7
	SPC/E	8.2 ± 0.8 (7.8 ± 0.3)	6.2 ± 0.8 (6.9 ± 0.4)	2.0 ± 1.1 (0.9 ± 0.5)
ff03	TIP3P	7.8 ± 0.6 (7.2 ± 0.3)	4.5 ± 0.6 (7.3 ± 0.3)	3.3 ± 0.8 (-0.1 ± 0.4)
	TIP4P	7.1 ± 0.4	6.3 ± 0.4	0.9 ± 0.5
	TIP5P	8.2 ± 0.8	5.6 ± 1.0	2.6 ± 1.3
	SPC/E	7.0 ± 0.3 (7.0 ± 0.2)	6.5 ± 0.4 (6.1 ± 0.2)	0.6 ± 0.5 (0.8 ± 0.3)

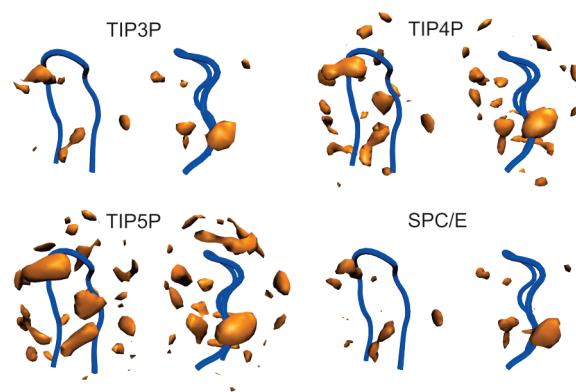
<sup>a</sup> The estimates in parentheses relate to 1  $\mu$ s long simulations.**Table 5.** Population (%) of the Native-like Chignolin Structure and Relative Populations (%) of Unfolded Chignolin Clusters in Multiple ff99 Simulations with the TIP3P, TIP4P, TIP5P, and SPC/E Models<sup>a</sup>

cluster number	TIP3P <sup>b</sup>	TIP4P <sup>b</sup>	TIP5P <sup>b</sup>	SPC/E <sup>b</sup>	TIP3P <sup>c</sup>	SPC/E <sup>c</sup>
native-like	18 ± 26	24 ± 26	53 ± 36	36 ± 35	3	11
1	67 ± 19	44 ± 31	5 ± 4	19 ± 32	72	71
2	8 ± 5	9 ± 15	50 ± 29	30 ± 35	0	10
3	1 ± 1	4 ± 5	8 ± 10	22 ± 37	1	1
4	19 ± 13	32 ± 39	24 ± 9	12 ± 13	12	6
5	9 ± 12	14 ± 21	17 ± 16	22 ± 36	13	12

<sup>a</sup> Note that the population of unfolded clusters is normalized, so it represents the portion of unfolded states. <sup>b</sup> Six independent simulations; the percentages of native-like structures and misfolded chignolin clusters of particular simulation runs are listed in Table S1 (Supporting Information). <sup>c</sup> A 1  $\mu$ s MD simulation.

Information). All simulations showed that the residues Thr6 and Glu5 could be found not only in the native right-handed  $\alpha$ -helical region, but also in a region of noncanonical artificial structures ( $\varphi = \sim -145^\circ$  and  $\psi = \sim 0^\circ$ ), which is a known artifact of ff99.<sup>18</sup> The most flexible Gly7 readily lost its native left-handed  $\alpha$ -helical conformation in TIP3P, TIP4P, and (eventually) SPC/E simulations and shifted to the artificial region around  $\varphi = \sim -165^\circ$  and  $\psi = \sim 35^\circ$  or to the glycine  $\beta_s$  region.<sup>62</sup> The population of the non-native and artificial region ( $\varphi = \sim -145^\circ$  and  $\psi = \sim 0^\circ$ ) was significantly reduced in TIP5P simulations, due to either slightly higher stability of chignolin in the TIP5P model or its favoring of cluster 2, causing less dense population of this artificial region.

**ff99SB Force Field.** In contrast to the ff99 simulations, chignolin was highly stable in all ff99SB simulations (Table 3). In most simulations, no unfolding event occurred, and even if the structure melted, it adopted near-native structures that swiftly refolded to the native chignolin. Both increased unfolding and decreased refolding free energy barriers contributed to significantly higher stability of the chignolin native structure in ff99SB simulations. On the other hand, neither stability nor estimated free energy barriers of unfolding and refolding differed in the set of four explicit solvent models (Table 4). The artificial population of the non-native region ( $\varphi = \sim -145^\circ$  and  $\psi = \sim 0^\circ$ ) of the Ramachandran

**Figure 2.** Water density maps (orange) around chignolin (the blue tube represents the chignolin backbone) for ff99SB simulations.

plots vanished in all ff99SB simulations, and backbone torsions of chignolin residues fluctuated around the NMR native values (Figure S5, Supporting Information).

The finding that chignolin was highly stable in all ff99SB simulations allowed us to monitor the behavior of water molecules in the vicinity of chignolin and to consider the effects of various solvent models on the specific solvation of chignolin. Both thermodynamic (the number and position of binding sites of long-residency water molecules) and kinetic (the mobility of these long-residency water molecules) perspectives on the preferential hydration of the chignolin surface were taken into account.<sup>63</sup> Similar local densities of water molecules were observed for simulations with the TIP4P and TIP5P models, while identifying large numbers of specific hydration sites. The three-site TIP3P and SPC/E water models also yielded similar density maps, but with significantly fewer specific hydration sites and with lower densities, in comparison with the TIP4P and TIP5P models (Figure 2). In addition, the analysis of long-residency water molecules (here, those with residence times longer than 0.5 ns) identified significant differences among solvation models, such that the number of long-residency water molecules decreased in the order TIP5P  $\gg$  SPC/E  $\approx$  TIP4P  $>$  TIP3P (Table 6).

These findings show that the specific hydration of chignolin is determined by the mobility of a given water model in terms of its self-diffusion coefficient (Table 1) and its

**Table 6.** Average Number of Water Molecules in the First Two Solvation Shells of Chignolin and Average Number of Long-Residency Water Molecules (Residence Times >0.5 ns) in ff99SB Chignolin Simulations with Corresponding Standard Deviations

	TIP3P	TIP4P	TIP5P	SPC/E	TIP3P <sup>1 μs</sup>	SPC/E <sup>1 μs</sup>
first shell, <3.4 Å	93 ± 8	93 ± 6	100 ± 8	94 ± 7	90 ± 6	95 ± 8
second shell, <5.0 Å	185 ± 14	182 ± 12	196 ± 15	186 ± 13	179 ± 11	189 ± 15
long-residency water molecules	0.0 ± 0.0	2.0 ± 1.3	12.8 ± 4.5	3.7 ± 2.7		

propensity to bind to specific hydration sites. Thus, the highest specific solvation in TIP5P simulations was caused by a large number of specific hydration sites and the low (and most realistic) mobility of TIP5P water molecules. On the other hand, no long-residency water molecules were identified for the TIP3P model, due to the small number of preferred hydration sites and rapid exchange of TIP3P water molecules at these sites. Interestingly, although the SPC/E model has a self-diffusion coefficient similar to that of TIP5P, the significantly smaller quantity of long-residency SPC/E water molecules was caused by a low number of specific hydration sites, most likely stemming from solute–solvent interactions and thermodynamic factors. Similarly, although the water density map of TIP4P was similar to that of TIP5P, with the same number of specific hydration sites, the higher self-diffusion coefficient of TIP4P resulted in significantly more rapid dynamics at these hydration sites, and thus, the specific hydration was reduced for kinetic reasons.

**ff03 Force Field.** As in ff99SB simulations, the chignolin native structure was highly populated in ff03 simulations. The rare unfolding events were frequently quickly followed by chignolin refolding in almost all cases, except in some SPC/E and TIP4P simulations and the 1 μs TIP3P simulation, where we observed minor but apparent populations of unfolded chignolin with Gly7 shifted from the left-handed α-helical region to the β<sub>PR</sub> region with φ = ~80° and ψ = ~-150° (Table 3; Figure S6, Supporting Information).<sup>62</sup> These non-native chignolin conformations closely match the β-hairpin topology, but lack the native hydrogen bond network and contacts between Tyr2 and Trp9 residues. On the other hand, the shift of Gly7 to the β<sub>PR</sub> region was always fully reversible, and refolding was sooner or later observed. It seems that the shift of Gly7 does not depend on the solvation model and can be considered as an ff03 force field effect. The difference in the balance between left-handed α-helical and β<sub>PR</sub> conformations of Gly7 in the ff03 and ff99SB force fields can be explained by differences in the free energy landscapes of the φ and ψ dihedrals in ff03 and ff99SB.<sup>45</sup>

**EK-Peptide, ff99 Force Field.** The EK-peptide readily lost its α-helical structure in all ff99 simulations (Table 3). Melting that propagated from the termini occurred within a time scale of hundreds of picoseconds to several nanoseconds. Melting times were progressively longer in the TIP5P and SPC/E water models, whose self-diffusion coefficients were smaller (and more realistic) than those of TIP3P, which had the highest self-diffusion coefficient of the explicit models in this study (Figures S13 and S14, Supporting Information). In the unfolded state, the peptide was highly dynamic, often switching among the <sub>310</sub>-helical structure, turn, random coil, and α-helical conformations. Some

**Table 7.** Salt Bridge Probabilities (Distance up to 4.5 Å) Calculated from EK-Peptide Simulations with ff03<sup>a</sup>

water model	Glu3...Lys6	Lys6...Glu9	Glu9...Lys12
TIP3P	0.36 ± 0.04 (0.35)	0.06 ± 0.02 (0.06)	0.31 ± 0.02 (0.33)
TIP4P	0.33 ± 0.07	0.03 ± 0.01	0.36 ± 0.04
TIP5P	0.49 ± 0.20	0.08 ± 0.10	0.51 ± 0.15
SPC/E	0.33 ± 0.07 (0.29)	0.06 ± 0.06 (0.06)	0.36 ± 0.07 (0.29)

<sup>a</sup> The mean probabilities and corresponding standard deviations were calculated from multiple simulations having helicity above 70%. The estimates in parentheses relate to 1 μs simulations.

residues also populated the artificial region around φ = ~-145° and ψ = ~0°, which is a known artifact of the ff99 force field.<sup>18</sup> Notably, internal residues of the EK-peptide had a propensity to refold for up to ~10 ns in the TIP5P and SPC/E models.

**ff99SB Force Field.** As in the previous case, the native α-helical fold was unstable throughout the time scale of the conducted simulations (Figures S15 and S16, Supporting Information). Melting of the helical structure occurred early, within a time scale of several nanoseconds, in simulations with the most mobile models, TIP3P and TIP4P. In contrast, in simulations using the water models with lower (and more realistic) mobility, TIP5P and SPC/E, the system melted later, generally on a time scale of tens of nanoseconds. The residues of the unfolded EK-peptide populated the left- and right-handed helical regions, the region of noncanonical structures around φ = ~-145° and ψ = ~0°, and the antiparallel β-sheet and triple-stranded collagen helix regions of the Ramachandran plot (Figures S8 and S11, Supporting Information). Nonetheless, the 1 μs TIP3P and SPC/E MD runs characterized the behavior of the system after melting, revealing that the antiparallel β-sheet, triple-stranded collagen helix, and left-handed regions were significantly populated in this state.

**ff03 Force Field.** In all simulations, the EK-peptide displayed a significant level of intrinsic α-helicity lying in the interval from ~70% to ~80% (Table 3; Figures S17 and S18, Supporting Information). The terminal residues had less helical propensity than internal residues and in the nonhelical state populated the triple-stranded collagen helix, antiparallel β-sheet, left-handed α-helix, and φ = ~-160° and ψ = ~-25° regions (Figures S9 and S12, Supporting Information).

The high stability of α-helical content in ff03 simulations of EK-peptide led us to monitor the stability of salt bridges between Lys and Glu side chains (Table 7) and the specific hydration of backbone carbonyl oxygen atoms (Figure 3). The formation of salt bridges and shielding of backbone H-bonds forming group (–C=O, –N–H) from water molecules were suggested to contribute to the stability of



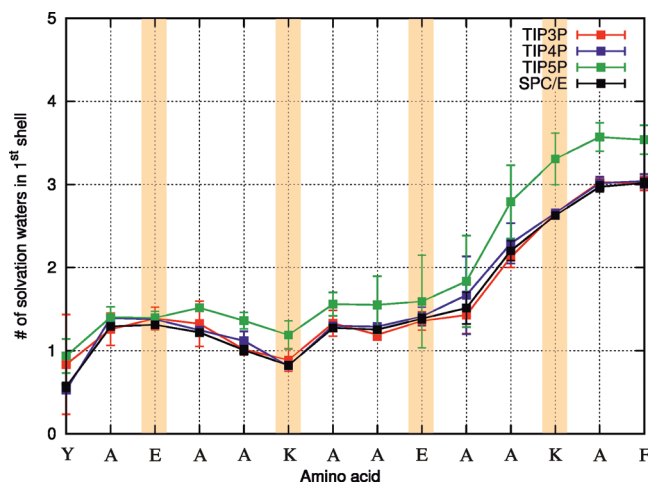


**Figure 3.** Average numbers of water molecules within the first hydration shell ( $<3.4$  Å) of backbone carbonyl oxygen atoms calculated from ff03 simulations of EK-peptide.

alanine-based  $\alpha$ -helical peptides (see refs 64 and 65 and references therein). The TIP3P, TIP4P, and SPC/E models behave similarly; i.e., the stability of salt bridges and hydration of backbone carbonyl oxygen atoms do not significantly differ among these three solvent models. On the other hand, MD simulations with TIP5P show higher stabilities of salt bridges (Table 7) and more extensive hydration of backbone carbonyl oxygen atoms (Figure 3).

## Discussion

In the present study we aimed to elucidate the effects of four popular explicit solvent models (TIP3P, TIP4P, TIP5P, and SPC/E) on the behavior of two oligopeptides: a  $\beta$ -hairpin chignolin and an  $\alpha$ -helical EK-peptide. We combined these solvent models with three recent protein force fields (ff99, ff99SB, and ff03) from the AMBER family. Our results suggest that the choice of solvent model does not significantly affect the stability of the studied peptides, which was completely governed by the force field employed. Furthermore, even the conformational behavior of the peptides in their native folded state was not influenced by the choice of solvent model.

We found that the ff99 force field destabilized the native fold of both peptides to an extent that significantly underestimated peptide stabilities in comparison with experimentally observed values.<sup>48,50</sup> In addition, in ff99 simulations we observed a significant population of noncanonical conformations in the form of  $\varphi$ - $\psi$  torsions ( $\varphi = \sim -145^\circ$  and  $\psi = \sim 0^\circ$ ), which are a known ff99 force field artifact.<sup>18</sup> Elimination of this artifact motivated the development of a reparametrized force field named ff99SB.<sup>18</sup> The ff99SB force field overstabilized the chignolin structure, while it did not improve the stability of the EK-peptide, destabilizing helical EK-peptide in favor of  $\beta$ -structured states. This indicates that although the ff99SB force field slightly improves the behavior of  $\beta$ -structured chignolin, it yields unbalanced force fields biased toward  $\beta$ -structures. Finally, the ff03 force field seemed the best choice among the tested force fields, as the chignolin stability estimated from all ff03 simulations was

$72 \pm 21\%$ , in good agreement with the experimentally observed chignolin stability of 60%. Moreover, the ff03 simulations did not cause any force field artifacts. They displayed folding/unfolding processes in chignolin connected with shifts of the flexible Gly7 between the left-handed  $\alpha$ -helix and  $\beta_{PR}$  conformations, which represents the tolerated conformational variability of this Gly residue. Nonetheless, the ff03 force field still overestimated the stability of  $\alpha$ -helical EK-peptide, as the  $\alpha$ -helicity observed in the ff03 simulations amounted to  $\sim 70$ – $80\%$ , while the experimental helical content equals  $\sim 20\%$  at 300 K. Thus, the ff03 force field seems the best, but still not perfect, choice from the studied set.

While we did not observe any effect of explicit solvent models on the stability of the studied peptides, we found substantial differences in specific solvation of the backbone carbonyls of the EK-peptide  $\alpha$ -helix and of the chignolin native structure in the set of studied water models. The TIP5P model showed more extensive hydration of backbone carbonyl oxygen atoms in comparison with TIP3P, TIP4P, and SPC/E, which gave almost the same results (Figure 3). The higher hydration of H-bonds between the backbone amide and carbonyl groups of the  $\alpha$ -helix was suggested to destabilize the  $\alpha$ -helicity of alanine-based peptides.<sup>64,65</sup> Thus, the lower  $\alpha$ -helicity of EK-peptide in the TIP5P simulations in comparison with other solvation models was anticipated as an effect of the more extensive backbone hydration. However, the  $\alpha$ -helicity of EK-peptide did not significantly differ among various solvent models (Table 3). This finding can be most likely explained by the higher probabilities of salt bridges in TIP5P water (Table 7) and compensation between the specific solvation of backbone carbonyl oxygens and salt bridge stabilities.

Chignolin was highly solvated in the TIP5P simulations, while significantly lower solvation was observed in other water model simulations. We analyzed the reasons for decreased specific solvation in the remaining three models and found that specific solvation by TIP4P was reduced by rapid exchange of water molecules in the solvation binding sites, i.e., for kinetic reasons. This finding can be explained by the larger self-diffusion coefficient of TIP4P in comparison with the TIP5P model. The specific solvation by SPC/E was reduced due to the small number of specific solvent binding sites compared to those in the TIP5P and TIP4P models, i.e., for thermodynamic reasons. Finally, the reduced specific solvation in TIP3P simulations was a consequence of both the aforementioned kinetic and thermodynamic factors (Figure 4). Consequently, assuming that the studied solvation models differ significantly in the specific solvation of solute and do not concurrently affect the stability of the studied peptide solutes, the question arises of whether these differences in specific solvation can influence the solute and, if so, how.

As the differences in specific solvation of the studied models did not affect the behavior of the studied peptides in their folded states, we focused rather on their behavior in unfolded states in ff99 simulations. We found that the conformational behavior of chignolin in unfolded states is similar in all three water models with lower specific solvation, i.e., in TIP3P, TIP4P, and SPC/E, while a different



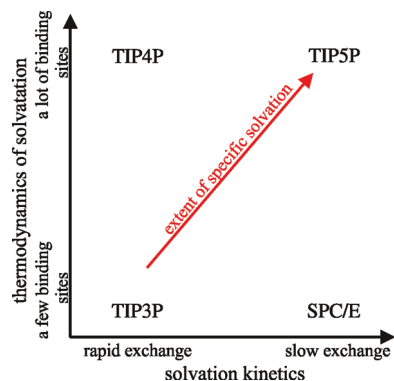


**Figure 4.** Schematic relationship among the solvation kinetics, thermodynamics of specific solvation (expressed by the number of specific binding sites), and extent of specific solvation of chignolin peptide in four studied water models.

conformational behavior of unfolded chignolin was observed in simulations with TIP5P, demonstrating a high degree of specific solvation. Specifically, we observed different preferences in the population of clusters of unfolded structures. The TIP3P, TIP4P, and SPC/E simulations resulted in preferred occupancy of the unfolded cluster with an artificial conformation of Gly7 ( $\varphi = \sim -165^\circ$  and  $\psi = \sim 35^\circ$ ), while in TIP5P simulations an alternative cluster with a left-handed  $\alpha$ -helical conformation of Gly7 was preferred. This result implies that the solvation models will most likely not significantly affect the structure, stability, and flexibility of structured segments of folded proteins. However, the differences in specific solvation might contribute to conformational variability and flexibility of solvent-exposed flexible parts, such as flexible glycine-rich loops. Notably, these most flexible parts of proteins are frequently connected with specific biological functions and are at the focus of attention of many MD simulations.<sup>51,52,66–72</sup> Moreover, specific solvation is also the subject of many other studies concerning, e.g., drug design.<sup>67,73–75</sup> Therefore, in these cases, the correct description of specific solvation might be critical for correct results.

Unfortunately, we are not able to ultimately conclude which model provides the most realistic description of specific solvation. On the other hand, our data suggest that the TIP5P model provides a significantly different specific solvation that could propagate to solute behavior via stability of salt bridges and modification of conformational preferences in unfolded states. As the TIP5P model has the most realistic solvent parameters (among studied solvent models), we suggest that TIP5P is the most promising candidate for the realistic description of solute–solvent interactions and specific solvation. Nonetheless, this implication is not straightforward and might be questionable, so direct comparison with reference experimental data of the specific solvation or of the solute–solvent interaction is needed to determine which model performs the best.

In addition, we observed a relationship between the mobility of a water model, represented by its self-diffusion coefficient, and the speed of processes in our simulations, namely, the kinetics of conversion between the unfolded clusters and the structural relaxation of unfolded states in

ff99 simulations. Thus, we conclude that the mobility of solvent models can accelerate the kinetics of processes in solutes.

Taken together, in sharp contrast to the choice of force field, choosing the most reliable water model is not straightforward. In cases where it can be assumed that specific solvation will not play an important role (i.e., in well-structured proteins lacking highly flexible loops), all the model performances may be similar in quality. Furthermore, in such cases, simulations can benefit from the high (overestimated) mobility of the TIP3P model, because it does not significantly affect the thermodynamic properties of the solutes, such as the structure of thermodynamically stable conformers, but it significantly reduces the barriers between these states and thus accelerates the kinetics and effectively increases sampling in the simulations. On the other hand, if the solute contains flexible and solvent-exposed loops, it would be better to use the more realistic description of solvation by the TIP5P model, even though this would entail an increased simulation time due to the relatively slower processes and lower sampling.

**Acknowledgment.** Support through the Ministry of Youth, Sports and Education of the Czech Republic (Grants CZ.1.05/2.1.00/03.0058, LC512, and MSM6198959216), the Grant Agency of the Czech Republic (Grant 203/09/H046), and Student Project PrF\_2010\_025 of Palacký University is gratefully acknowledged. We thank Sees-Editing, Ltd. (U.K.) for linguistic revision.

**Supporting Information Available:** Figures S1–S21 and Tables S1–S4 giving the OO radial distribution function for explicit water models, three-dimensional structure and scatter plots of chignolin misfolded structures (ff99) and scatter plot of chignolin NMR structures, time courses of rmsd colored according to chignolin misfolded structures (ff99), population of the chignolin clusters and populations of the native-like chignolin structures in TIP3P, TIP4P, TIP5P, and SPC/E models for chignolin simulations, Ramachandran density and scatter plots of chignolin simulations, secondary structure of EK-peptide simulations, Ramachandran density and scatter plots of EK-peptide long simulations, secondary structure of EK-peptide (ff99SB), secondary structure of EK-peptide (ff03),  $\alpha$ -helicity of EK-peptide, salt-bridge probabilities (ff03), normalized histograms of Lys–Glu distances, cumulative histograms of the probability of salt-bridge formation, and number of waters within the first hydration shell around the carbonyl oxygen of each residue in the EK-peptide (ff03). This material is available free of charge via the Internet at <http://pubs.acs.org>.

## References

- (1) Mackerell, A. D. *J. Comput. Chem.* **2004**, *25*, 1584.
- (2) Ponder, J. W.; Case, D. A. *Adv. Protein Chem.* **2003**, *66*, 27.
- (3) van der Kamp, M. W.; Shaw, K. E.; Woods, C. J.; Mulholland, A. J. *J. R. Soc. Interface* **2008**, *5* (3), S173.
- (4) van Gunsteren, W. F.; Bakowies, D.; Baron, R.; Chandrasekhar, I.; Christen, M.; Daura, X.; Gee, P.; Geerke,

- D. P.; Glattli, A.; Hunenberger, P. H.; Kastenholz, M. A.; Oostenbrink, C.; Schenk, M.; Trzesniak, D.; van der Vegt, N. F.; Yu, H. B. *Angew. Chem., Int. Ed.* **2006**, *45*, 4064.
- (5) Spöner, J.; Spackova, N. *Methods* **2007**, *43*, 278.
- (6) Pearlman, D. A.; Case, D. A.; Caldwell, J. W.; Ross, W. S.; Cheatham, T. E.; Debolt, S.; Ferguson, D.; Seibel, G.; Kollman, P. *Comput. Phys. Commun.* **1995**, *91*, 1.
- (7) Case, D. A.; Cheatham, T. E.; Darden, T.; Gohlke, H.; Luo, R.; Merz, K. M.; Onufriev, A.; Simmerling, C.; Wang, B.; Woods, R. J. *J. Comput. Chem.* **2005**, *26*, 1668.
- (8) Berendsen, H. J. C.; Vanderspoel, D.; Vandrunen, R. *Comput. Phys. Commun.* **1995**, *91*, 43.
- (9) Brooks, B. R.; Brucoleri, R. E.; Olafson, B. D.; States, D. J.; Swaminathan, S.; Karplus, M. *J. Comput. Chem.* **1983**, *4*, 187.
- (10) Kaminski, G. A.; Friesner, R. A.; Tirado-Rives, J.; Jorgensen, W. L. *J. Phys. Chem. B* **2001**, *105*, 6474.
- (11) Guvench, O.; MacKerell, A. D., Jr. *Methods Mol. Biol.* **2008**, *443*, 63.
- (12) Ditzler, M. A.; Otyepka, M.; Spöner, J.; Walter, N. G. *Acc. Chem. Res.* **2010**, *43*, 40.
- (13) Perez, A.; Lankas, F.; Luque, F. J.; Orozco, M. *Nucleic Acids Res.* **2008**, *36*, 2379.
- (14) Lavery, R.; Zakrzewska, K.; Beveridge, D.; Bishop, T. C.; Case, D. A.; Cheatham, T., III; Dixit, S.; Jayaram, B.; Lankas, F.; Laughton, C.; Maddocks, J. H.; Michon, A.; Osman, R.; Orozco, M.; Perez, A.; Singh, T.; Spackova, N.; Spöner, J. *Nucleic Acids Res.* **2010**, *38*, 299.
- (15) MacKerell, A. D.; Nilsson, L. *Curr. Opin. Struct. Biol.* **2008**, *18*, 194.
- (16) Wang, J. M.; Cieplak, P.; Kollman, P. A. *J. Comput. Chem.* **2000**, *21*, 1049.
- (17) Cieplak, P.; Cornell, W. D.; Bayly, C.; Kollman, P. A. *J. Comput. Chem.* **1995**, *16*, 1357.
- (18) Hornak, V.; Abel, R.; Okur, A.; Strockbine, B.; Roitberg, A.; Simmerling, C. *Proteins* **2006**, *65*, 712.
- (19) Duan, Y.; Wu, C.; Chowdhury, S.; Lee, M. C.; Xiong, G. M.; Zhang, W.; Yang, R.; Cieplak, P.; Luo, R.; Lee, T.; Caldwell, J.; Wang, J. M.; Kollman, P. *J. Comput. Chem.* **2003**, *24*, 1999.
- (20) Best, R. B.; Buchete, N. V.; Hummer, G. *Biophys. J.* **2008**, *95*, 4494.
- (21) Best, R. B.; Hummer, G. *J. Phys. Chem. B* **2009**, *113*, 9004.
- (22) Chandler, D. *Nature* **2005**, *437*, 640.
- (23) Roca, M.; Messer, B.; Warshel, A. *FEBS Lett.* **2007**, *581*, 2065.
- (24) Warshel, A.; Sharma, P. K.; Kato, M.; Parson, W. W. *Biochim. Biophys. Acta* **2006**, *1764*, 1647.
- (25) Leach, A. R. *Molecular Modelling: Principles and Applications*, 2nd ed.; Prentice Hall: Upper Saddle River, NJ, 2001; p 768.
- (26) Orozco, M.; Luque, F. J. *Chem. Rev.* **2000**, *100*, 4187.
- (27) Guillot, B. *J. Mol. Liq.* **2002**, *101*, 219.
- (28) Mahoney, M. W.; Jorgensen, W. L. *J. Chem. Phys.* **2000**, *112*, 8910.
- (29) Mahoney, M. W.; Jorgensen, W. L. *J. Chem. Phys.* **2001**, *114*, 363.
- (30) Kusalik, P. G.; Svishchev, I. M. *Science* **1994**, *265*, 1219.
- (31) Vega, C.; Abascal, J. L. F. *J. Chem. Phys.* **2005**, *123*, 144504.
- (32) Vega, C.; Sanz, E.; Abascal, J. L. F. *J. Chem. Phys.* **2005**, *122*, 114507.
- (33) Baez, L. A.; Clancy, P. J. *J. Chem. Phys.* **1994**, *101*, 9837.
- (34) Vega, C.; McBride, C.; Sanz, E.; Abascal, J. L. F. *Phys. Chem. Chem. Phys.* **2005**, *7*, 1450.
- (35) Mark, P.; Nilsson, L. *J. Phys. Chem. A* **2001**, *105*, 9954.
- (36) Zielkiewicz, J. *J. Chem. Phys.* **2005**, *123*, 104501.
- (37) Hess, B.; van der Vegt, N. F. *J. Phys. Chem. B* **2006**, *110*, 17616.
- (38) Jorgensen, W. L.; Chandrasekhar, J.; Madura, J. D.; Impey, R. W.; Klein, M. L. *J. Chem. Phys.* **1983**, *79*, 926.
- (39) Berendsen, H. J. C.; Grigera, J. R.; Straatsma, T. P. *J. Phys. Chem.* **1987**, *91*, 6269.
- (40) Nutt, D. R.; Smith, J. C. *J. Chem. Theory Comput.* **2007**, *3*, 1550.
- (41) Shirts, M. R.; Pande, V. S. *J. Chem. Phys.* **2005**, *122*, 1.
- (42) Wong, V.; Case, D. A. *J. Phys. Chem. B* **2008**, *112*, 6013.
- (43) Glass, D. C.; Krishnan, M.; Nutt, D. R.; Smith, J. C. *J. Chem. Theory Comput.* **2010**, *6*, 1390.
- (44) Price, D. J.; Brooks, C. L. *J. Chem. Phys.* **2004**, *121*, 10096.
- (45) Vymetal, J.; Vondrasek, J. *J. Phys. Chem. B* **2010**, *114*, 5632.
- (46) Sun, Y. X.; Kollman, P. A. *J. Comput. Chem.* **1995**, *16*, 1164.
- (47) Shirts, M. R.; Pitera, J. W.; Swope, W. C.; Pande, V. S. *J. Chem. Phys.* **2003**, *119*, 5740.
- (48) Honda, S.; Yamasaki, K.; Sawada, Y.; Morii, H. *Structure* **2004**, *12*, 1507.
- (49) Scholtz, J. M.; Barrick, D.; York, E. J.; Stewart, J. M.; Baldwin, R. L. *Proc. Natl. Acad. Sci. U.S.A.* **1995**, *92*, 185.
- (50) Ghosh, K.; Dill, K. A. *J. Am. Chem. Soc.* **2009**, *131*, 2306.
- (51) Bartova, I.; Koca, J.; Otyepka, M. *J. Mol. Model.* **2008**, *14*, 761.
- (52) Wilson, E. B. *J. Am. Stat. Assoc.* **1927**, *22*, 209.
- (53) Sklenovsky, P.; Banas, P.; Otyepka, M. *J. Mol. Model.* **2008**, *14*, 747.
- (54) Skopalik, J.; Anzenbacher, P.; Otyepka, M. *J. Phys. Chem. B* **2008**, *112*, 8165.
- (55) Sklenovsky, P.; Otyepka, M. *J. Biomol. Struct. Dyn.* **2010**, *27*, 521.
- (56) Berendsen, H. J. C.; Postma, J. P. M.; Vangunsteren, W. F.; Dinola, A.; Haak, J. R. *J. Chem. Phys.* **1984**, *81*, 3684.
- (57) Day, R.; Daggett, V. *Proc. Natl. Acad. Sci. U.S.A.* **2005**, *102*, 13445.
- (58) Scott, K. A.; Alonso, D. O. V.; Pan, Y. P.; Daggett, V. *Biochemistry* **2006**, *45*, 4153.
- (59) Shao, J. Y.; Tanner, S. W.; Thompson, N.; Cheatham, T. E. *J. Chem. Theory Comput.* **2007**, *3*, 2312.
- (60) Schlick, T. *Molecular Modeling and Simulation: An Interdisciplinary Guide*; Springer Science + Business Media LLC: New York, 2002; Vol. 21.
- (61) Kriz, Z.; Otyepka, M.; Bartova, I.; Koca, J. *Proteins* **2004**, *55*, 258.
- (62) Ho, B. K.; Brasseur, R. *BMC Struct. Biol.* **2005**, *5*, 14.

- (63) Priya, M. H.; Shah, J. K.; Asthagiri, D.; Paulaitis, M. E. *Biophys. J.* **2008**, 95, 2219.
- (64) Garcia, A. E.; Sanbonmatsu, K. Y. *Proc. Natl. Acad. Sci. U.S.A.* **2002**, 99, 2782.
- (65) Ghosh, T.; Garde, S.; Garcia, A. E. *Biophys. J.* **2003**, 85, 3187.
- (66) Dvorakova-Hola, K.; Matuskova, A.; Kubala, M.; Otyepka, M.; Kucera, T.; Vecer, J.; Herman, P.; Parkhomenko, N.; Kutejova, E.; Janata, J. *J. Mol. Biol.* **2010**, 396, 1197.
- (67) Bartova, I.; Otyepka, M.; Kriz, Z.; Koca, J. *Protein Sci.* **2005**, 14, 445.
- (68) Bartova, I.; Otyepka, M.; Kriz, Z.; Koca, J. *Protein Sci.* **2004**, 13, 1449.
- (69) Wong, L.; Jennings, P. A.; Adams, J. A. *Acc. Chem. Res.* **2004**, 37, 304.
- (70) Narayanan, A.; Jacobson, M. P. *Curr. Opin. Struct. Biol.* **2009**, 19, 156.
- (71) Prudent, R.; Sautel, C. F.; Cochet, C. *BBA—Proteins Proteomics* **2010**, 1804, 493.
- (72) Otyepka, M.; Bartova, I.; Kriz, Z.; Koca, J. *J. Biol. Chem.* **2006**, 281, 7271.
- (73) de Beer, S. B.; Vermeulen, N. P.; Oostenbrink, C. *Curr. Top. Med. Chem.* **2010**, 10, 55.
- (74) Yan, A.; Grant, G. H.; Richards, W. G. *J. R. Soc. Interface* **2008**, 5 (3), S199.
- (75) Zhang, B.; Tan, V. B.; Lim, K. M.; Tay, T. E. *J. Chem. Inf. Model.* **2007**, 47, 1877.
- (76) Hasted, J. B. Liquid Water: Dielectric Properties. *Water: A Comprehensive Treatise*; Plenum Press: New York, 1972; Vol. 1.
- (77) Gubskaya, A. V.; Kusalik, P. G. *J. Chem. Phys.* **2002**, 117, 5290.
- (78) Fernandez, D. P.; Mulev, Y.; Goodwin, A. R. H.; Sengers, J. M. H. L. *J. Phys. Chem. Ref. Data* **1995**, 24, 33.
- (79) Jancso, G.; van Hook, W. A. *Chem. Rev.* **1974**, 74, 689.

CT1003687